Accurate static response of single- and multi-cell laminated box beams

Accurate static response of single- and multi-cell laminated box beams

E. Carrera[a*], M. Filippi[a†], P.K. Mahato[a,b‡], A. Pagani[a§]

[a]Department of Mechanical and Aerospace Engineering, Politecnico di Torino,
Corso Duca degli Abruzzi 24, 10129 Torino, Italy.

[b]Department of Mechanical Engineering,
Indian School of Mines, Dhanbad-826004, India.

Abstract

This paper is devoted to the static analysis of laminated beams with both compact and thin-walled cross-sections. The kinematic models are obtained by means of the Carrera Unified Formulation (CUF), which is a hierarchical formulation leading to very accurate and computationally efficient finite element (FE) models. According to the latest developments in the framework of CUF, it is possible to easily adopt both equivalent-single-layer and layer-wise approaches, by expanding the unknown kinematic variables on the beam cross-section with either Taylor-like or Lagrange-like polynomials, respectively. A number of laminated beam structures are analysed and particular attention is given to laminated single- and multi-cell cross-section beams with open and closed contours. Moreover, in order to demonstrate the effectiveness of the proposed refined elements, the results in terms of displacements and stresses are compared with solid FE solutions and, when possible, with the results available from the research literature.

Keywords: Refined Theories, Finite Element Method, Carrera Unified Formulation, Laminated Beams, Box Beams, Composites.

1. Introduction

Many engineering applications require structures whose stiffness-to-weight ratio must comply stringent specifications, thus thin-walled profiles made of laminated composite materials represent efficient constructive solutions. Although the analysis and the prediction of the mechanical behavior of this kind of structures are extremely complex processess to undertake, a considerable number of analytical as well as numerical methods have been proposed over the years. The

*Professor of Aerospace Structures and Aeroelasticity, e-mail: erasmo.carrera@polito.it
†Research Fellow, e-mail: matteo.filippi@polito.it
‡Visiting Scientist, e-mail: prashanta.mahato@polito.it
§Research Fellow, e-mail: alfonso.pagani@polito.it

one-dimensional approach has played a very important role in the modelling of many weight-sensitive structures (such as wings and blades) due to its simplicity and low computational cost. However, the accuracy of the classical beam theories, proposed by Euler and Bernoully [1] and Timoshenko, [2] is questionable when the shear and the elastic coupling effects become relevant. This fact was clearly pointed out in [3], where Bachau *et al.* examined box laminated beams subjected to torsional loadings. In order to accurately describe the cross sectional deformation, the authors proposed two theoretical models in which different warping functions have been included. The theoretical predictions have been found in good agreement with experimental measurements. Another simple theoretical approach was later proposed by Loughlan *et al.* [4] in order to predict the torsional response of cantilever beams with symmetric laminated walls subjected to a torque at the free end. This analytical model makes used of suitably modified theories of torsion derived by those adopted for isotropic structures. Interesting considerations have been made on the primary and secondary warping of both open [4] and closed [5, 6, 7] profiles.

In order to overcome the limitations of the analytical models, for which loads and boundary conditions must be usually prescribed, several studies have been focused on the development of efficient finite elements. For instance, Stemple *et al.* [8] have conceived a refined beam element in which the transverse shear deformations and the cross-sectional warping have been included. A number of numerical tests have been firstly carried out on structures with thin-walled circular and elliptical cross-sections [8] and then on symmetric and antisymmetric lay-up composite box beams [9]. The results, which were compared with analytical and shell solutions as well as with experimental data, have proved the high efficiency of this formulation. According to the variational asymptotic method, Mira Mitra *et al.* [10] and Sheikh *et al.* [11] developed efficient beam elements in which non-classical effects have been considered, such as transverse shear, out-of-plane and torsional deformations. The validations of their approaches have been done through a number of static and dynamic analyses carried out on both open and closed beam profiles subjected to several constrained conditions. On the other hand, Vo *et al.* [12, 13, 14] focused their attentions on the study of the static, dynamic and stability behaviours of box beams. The authors developed Hermitian and Lagrangian elements based on the classical and

shear-deformable theories, respectively. The use of both formulations allowed them to predict the flexural-torsional response of symmetric and asymmetric laminated structures with a good accuracy. Suresh *et al.* [15] proposed a number of results related to the longitudinal stress distributions through the thickness of laminated boxes. Each wall of the box beam was modelled by using 2D finite elements based on Mindlin theory which takes shear deformation into consideration. The effects of materials and lay-up sequence were studied for a simply supported box beam under an uniformly distributed load. Further contributions in the study of light structures have been recently discussed in [16, 17], in which a Hellinger-Reissner mixed variational principle was adopted in order to independently interpolate the displacement and stress fields. Comparisons between the 1D mixed theory and the results from 3D finite element solutions have been shown to give close agreement.

The present paper aims at presenting 1D higher-order beam elements based on generalized displacement variables to carry out static analysis of laminated composite box beams. This work is the extension of a companion paper [18] about free vibration analyses of laminated composite box beams, in which two classes of CUF 1D models have been used. The Taylor-Expansion class [19], hereafter referred to as TE, exploit N-order Taylor-like polynomials to define the displacement field above the cross-section with N as a free parameter of the formulation. The capabilities of TE beam elements in dealing with arbitrary geometries, thin-walled structures and local effects were pointed out in static [20, 21] and free-vibration analyses [22, 23, 24]. Moreover, the TE theories have been recently applied in the Dynamic Stiffness method framework [25, 26] and in the study of the dynamics of composite rotors [27, 28, 29]. On the other hand, the Lagrange-Expansion class, hereafter referred to as LE, is based on Lagrange-like polynomials to discretize the cross-section displacement field and they have only pure displacement variables. Although the C_z^0-requirement through the thickness is only *a priori* fulfilled for the displacement field (see [30]), the LE elements have been able to provide accurate descriptions of the transverse stress distributions also for laminated structures [31]. The latest extensions of LE models have concerned the component-wise analyses of complex aeronautical [32, 33] and civil engineering structures [34, 35].

In this paper, the static response of a variety of thin-walled laminated beams with both open and

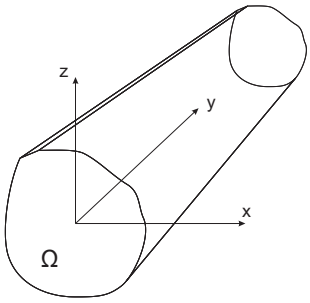

Figure 1: Coordinate frame of the beam model.

closed profiles has been examined and special attention has been paid to single- and multi-cell beams. Each beam wall is made of a number of orthotropic layers that are arbitrarily rotated about the longitudinal axis (that is the y-axis for the present reference system). The results in terms of displacements and stresses have revealed that the 1D CUF elements represent an efficient tool for the study of the thin-walled laminated structures.

2. Unified formulation

2.1. Preliminaries

The adopted coordinate frame is presented in Fig. 1. The beam boundaries over y are $0 \leq y \leq L$. The displacement vector is:

$$\mathbf{u}(x,y,z) = \left\{ \begin{array}{ccc} u_x & u_y & u_z \end{array} \right\}^T \tag{1}$$

Stress, $\boldsymbol{\sigma}$, and strain, $\boldsymbol{\epsilon}$, components are grouped as follows:

$$\begin{array}{l} \boldsymbol{\sigma}_p = \left\{ \begin{array}{ccc} \sigma_{zz} & \sigma_{xx} & \sigma_{zx} \end{array} \right\}^T, \quad \boldsymbol{\epsilon}_p = \left\{ \begin{array}{ccc} \epsilon_{zz} & \epsilon_{xx} & \epsilon_{zx} \end{array} \right\}^T \\ \boldsymbol{\sigma}_n = \left\{ \begin{array}{ccc} \sigma_{zy} & \sigma_{xy} & \sigma_{yy} \end{array} \right\}^T, \quad \boldsymbol{\epsilon}_n = \left\{ \begin{array}{ccc} \epsilon_{zy} & \epsilon_{xy} & \epsilon_{yy} \end{array} \right\}^T \end{array} \tag{2}$$

The subscript "n" stands for terms lying on the cross-section, while "p" stands for terms lying on planes which are orthogonal to Ω. Linear strain-displacement relations are used:

$$\begin{array}{l} \boldsymbol{\epsilon}_p = \boldsymbol{D}_p \mathbf{u} \\ \boldsymbol{\epsilon}_n = \boldsymbol{D}_n \mathbf{u} = (\boldsymbol{D}_{n\Omega} + \boldsymbol{D}_{ny}) \mathbf{u} \end{array} \tag{3}$$

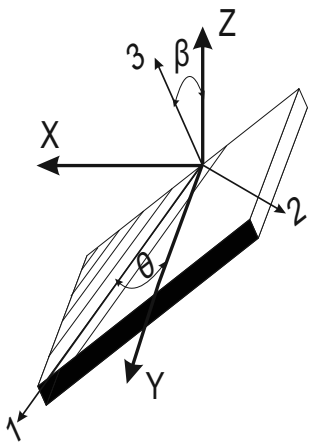

Figure 2: Physical and material reference systems

with:

$$\boldsymbol{D}_p = \begin{bmatrix} 0 & 0 & \frac{\partial}{\partial z} \\ \frac{\partial}{\partial x} & 0 & 0 \\ \frac{\partial}{\partial z} & 0 & \frac{\partial}{\partial x} \end{bmatrix}, \quad \boldsymbol{D}_{n\Omega} = \begin{bmatrix} 0 & \frac{\partial}{\partial z} & 0 \\ 0 & \frac{\partial}{\partial x} & 0 \\ 0 & 0 & 0 \end{bmatrix}, \quad \boldsymbol{D}_{ny} = \begin{bmatrix} 0 & 0 & \frac{\partial}{\partial y} \\ \frac{\partial}{\partial y} & 0 & 0 \\ 0 & \frac{\partial}{\partial y} & 0 \end{bmatrix} \tag{4}$$

The Hooke law is exploited:

$$\boldsymbol{\sigma} = \tilde{\boldsymbol{C}}\boldsymbol{\epsilon} \tag{5}$$

According to Eq. 2, the Eq. 5 becomes:

$$\begin{aligned} \boldsymbol{\sigma}_p &= \tilde{\boldsymbol{C}}_{pp}\boldsymbol{\epsilon}_p + \tilde{\boldsymbol{C}}_{pn}\boldsymbol{\epsilon}_n \\ \boldsymbol{\sigma}_n &= \tilde{\boldsymbol{C}}_{np}\boldsymbol{\epsilon}_p + \tilde{\boldsymbol{C}}_{nn}\boldsymbol{\epsilon}_n \end{aligned} \tag{6}$$

Box beams can be considered constituted by a certain number of straight orthotropic layers, whose material coordinate system $(1, 2, 3)$ generally do not coincide with the physical coordinate system (x, y, z) as shown in Fig. 2. This figure also shows the capability of the present formulation to deal with arbitrary rotations of the fibres both in *xy*- and *xz*-planes. Using this

approach, the matrices containing the coefficients of the generic material k are fully populated.

$$\tilde{\boldsymbol{C}}^k_{pp} = \begin{bmatrix} \tilde{C}^k_{11} & \tilde{C}^k_{12} & \tilde{C}^k_{14} \\ \tilde{C}^k_{12} & \tilde{C}^k_{22} & \tilde{C}^k_{24} \\ \tilde{C}^k_{14} & \tilde{C}^k_{24} & \tilde{C}^k_{44} \end{bmatrix}, \qquad \tilde{\boldsymbol{C}}^k_{pn} = \begin{bmatrix} \tilde{C}^k_{15} & \tilde{C}^k_{16} & \tilde{C}^k_{13} \\ \tilde{C}^k_{25} & \tilde{C}^k_{26} & \tilde{C}^k_{23} \\ \tilde{C}^k_{45} & \tilde{C}^k_{46} & \tilde{C}^k_{43} \end{bmatrix}$$
$$\tilde{\boldsymbol{C}}^k_{nn} = \begin{bmatrix} \tilde{C}^k_{55} & \tilde{C}^k_{56} & \tilde{C}^k_{35} \\ \tilde{C}^k_{56} & \tilde{C}^k_{66} & \tilde{C}^k_{36} \\ \tilde{C}^k_{35} & \tilde{C}^k_{36} & \tilde{C}^k_{33} \end{bmatrix} \tag{7}$$

The explicit forms of the coefficients of the matrices $\tilde{\boldsymbol{C}}^k_{ij}$ are not given here for the sake of brevity, but they can be found in [29].

2.2. Hierarchical Higher-Order Models, TE and LE Classes

In the framework of CUF, the displacement field is the expansion of generic cross-sectional functions, F_τ

$$\boldsymbol{u}(x, y, z) = F_\tau(x, z)\boldsymbol{u}_\tau(y) \qquad \tau = 1, 2, \ldots, M \tag{8}$$

where $\boldsymbol{u}_\tau$ is the vector of the *generalized* displacement, M is the number of terms of the expansion and, in according to the generalized Einstein's notation, τ indicates summation. The choice of F_τ determines the class of the 1D CUF model that has to be adopted. TE 1D models are based on polynomial expansions, $x^i z^j$, of the displacement field above the cross-section of the structure, where i and j are positive integers. For instance, the displacement field of the second-order (N=2) TE model is expressed by

$$\begin{aligned} u_x &= u_{x_1} + x\, u_{x_2} + z\, u_{x_3} + x^2\, u_{x_4} + xz\, u_{x_5} + z^2\, u_{x_6} \\ u_y &= u_{y_1} + x\, u_{y_2} + z\, u_{y_3} + x^2\, u_{y_4} + xz\, u_{y_5} + z^2\, u_{y_6} \\ u_z &= u_{z_1} + x\, u_{z_2} + z\, u_{z_3} + x^2\, u_{z_4} + xz\, u_{z_5} + z^2\, u_{z_6} \end{aligned} \tag{9}$$

The order N of the expansion is an input parameter of the analysis and defines the beam theory.

The LE class exploits Lagrange-like polynomials on the cross-section to build 1D higher-order models. The isoparametric formulation is exploited to deal with arbitrary shape geometries. In this paper, the nine-point (L9) cross-sectional polynomial set was adopted. For a L9

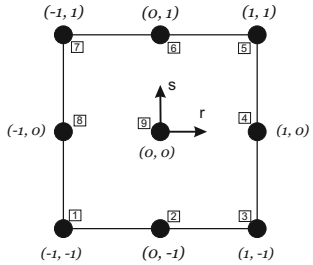

Figure 3: L9 element in the natural coordinate system

element (Fig. 3), the interpolation functions are given by

$$F_\tau = \tfrac{1}{4}(r^2 + r\ r_\tau)(s^2 + s\ s_\tau) \qquad \tau = 1, 3, 5, 7$$

$$F_\tau = \tfrac{1}{2}s_\tau^2(s^2 - s\ s_\tau)(1 - r^2) + \tfrac{1}{2}r_\tau^2(r^2 - r\ r_\tau)(1 - s^2) \qquad \tau = 2, 4, 6, 8 \tag{10}$$

$$F_\tau = (1 - r^2)(1 - s^2) \qquad \tau = 9$$

where r and s vary from -1 to $+1$, whereas r_τ and s_τ are the coordinates of the nine points whose locations in the natural coordinate frame are shown in Fig. 3. The displacement field of a L9 element is therefore

$$\begin{aligned} u_x &= F_1\ u_{x_1} + F_2\ u_{x_2} + F_3\ u_{x_3} + ... + F_9\ u_{x_9} \\ u_y &= F_1\ u_{y_1} + F_2\ u_{y_2} + F_3\ u_{y_3} + ... + F_9\ u_{y_9} \\ u_z &= F_1\ u_{z_1} + F_2\ u_{z_2} + F_3\ u_{z_3} + ... + F_9\ u_{z_9} \end{aligned} \tag{11}$$

where $u_{x_1}, ..., u_{z_9}$ are the displacement variables of the problem and they represent the translational displacement components of each of the nine points of the L9 element. According to [36], the beam cross-section can be discretized by using several L-elements for further refinements, as shown in Fig. 4 where two L9 elements are assembled. This is one of the main feature of the LE approach, which clearly has LW capabilities as discussed in [31].

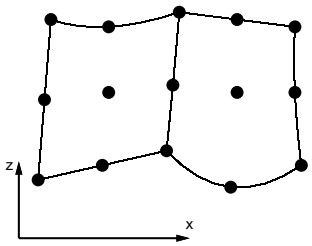

Figure 4: Two assembled L9 elements in actual geometry

2.3. FE formulation

The FE approach was adopted to discretize the structure along the y-axis. The displacement field is given by:

$$\boldsymbol{u}(x,y,z) = N_i(y)F_\tau(x,z)\mathbf{q}_{\tau i} \tag{12}$$

where N_i stands for (1D) shape functions and $\mathbf{q}_{\tau i}$ for the nodal displacement vector

$$\mathbf{q}_{\tau i} = \left\{ \begin{array}{ccc} q_{u_{x_{\tau i}}} & q_{u_{y_{\tau i}}} & q_{u_{z_{\tau i}}} \end{array} \right\}^T \tag{13}$$

For the sake of brevity, the shape functions are not reported here. They can be found in many books, for instance in [37]. The choice of the cross-section discretization for the LE class (i.e. the choice of the type, the number and the distribution of cross-sectional elements) or the theory order, N, for TE class is completely independent of the choice of the beam finite element to be used along the beam axis. In this work, 1D Lagrangian elements with four nodes (B4) were adopted, i.e. a cubic approximation along the *y*-axis was assumed.

The stiffness matrix of the elements and the external loadings, which are consistent with the model, are obtained via the principle of virtual displacements

$$\delta L_{int} = \int_V (\delta\boldsymbol{\epsilon}_p^T\boldsymbol{\sigma}_p + \delta\boldsymbol{\epsilon}_n^T\boldsymbol{\sigma}_n)dV = -\delta L_{ext} \tag{14}$$

where L_{int} stands for the strain energy and L_{ext} is the work of the external loadings. δ stands for the virtual variation. The virtual variation of the strain energy is rewritten using Eq.s (3), (6) and (12)

$$\delta L_{int} = \delta\mathbf{q}_{\tau i}^T\mathbf{K}^{ij\tau s}\mathbf{q}_{sj} \tag{15}$$

where $\mathbf{K}^{ij\tau s}$ is the stiffness matrix in the form of the fundamental nucleus. In a compact notation,

it can be written as

$$
\begin{aligned}
\boldsymbol{K}^{ij\tau s} = {}& I_l^{ij} \triangleleft (\boldsymbol{D}_{np}^T F_\tau \boldsymbol{I})\Big[\tilde{\boldsymbol{C}}_{np}^k (\boldsymbol{D}_p F_s \boldsymbol{I}) + \tilde{\boldsymbol{C}}_{nn}^k (\boldsymbol{D}_{np} F_s \boldsymbol{I})\Big] + \\
& (\boldsymbol{D}_p^T F_\tau \boldsymbol{I})\Big[\tilde{\boldsymbol{C}}_{pp}^k (\boldsymbol{D}_p F_s \boldsymbol{I}) + \tilde{\boldsymbol{C}}_{pn}^k (\boldsymbol{D}_{np} F_s \boldsymbol{I})\Big] \triangleright_\Omega + \\
& I_l^{ij,y} \triangleleft \Big[(\boldsymbol{D}_{np}^T F_\tau \boldsymbol{I})\tilde{\boldsymbol{C}}_{nn}^k + (\boldsymbol{D}_p^T F_\tau \boldsymbol{I})\tilde{\boldsymbol{C}}_{pn}^k\Big] F_s \triangleright_\Omega \boldsymbol{I}_{\Omega y} + \\
& I_l^{i,y j} \boldsymbol{I}_{\Omega y} \triangleleft F_\tau \Big[\tilde{\boldsymbol{C}}_{np}^k (\boldsymbol{D}_p F_s \boldsymbol{I}) + \tilde{\boldsymbol{C}}_{nn}^k (\boldsymbol{D}_{np} F_s \boldsymbol{I})\Big] \triangleright_\Omega + \\
& I_l^{i,y j_y} \boldsymbol{I}_{\Omega y} \triangleleft F_\tau \tilde{\boldsymbol{C}}_{nn}^k F_s \triangleright_\Omega \boldsymbol{I}_{\Omega y}
\end{aligned}
\tag{16}
$$

where

$$
\boldsymbol{I}_{\Omega y} = \begin{bmatrix} 0 & 1 & 0 \\ 1 & 0 & 0 \\ 0 & 0 & 1 \end{bmatrix} \qquad \triangleleft \ldots \triangleright_\Omega = \int_\Omega \ldots d\Omega \tag{17}
$$

$$
\left(I_l^{ij}, I_l^{ij,y}, I_l^{i,y j}, I_l^{i,y j_y}\right) = \int_l \left(N_i N_j,\ N_i N_{j,y},\ N_{i,y} N_j,\ N_{i,y} N_{j,y}\right) dy \tag{18}
$$

For the sake of clearness, in Appendix A, the nine components of the fundamental nucleus of the matrix $\boldsymbol{K}^{ij\tau s}$ are written in explicit form.

The variationally coherent loadings vector is derived in the case of a generic concentrated load **P**:

$$
\mathbf{P} = \left\{ \begin{array}{ccc} P_{u_x} & P_{u_y} & P_{u_z} \end{array} \right\}^T \tag{19}
$$

Any other loading condition can be similarly treated. The virtual work due to **P** is:

$$
\delta L_{ext} = \mathbf{P} \delta \mathbf{u}^T \tag{20}
$$

By introducing the nodal generalized displacements and the shape functions along with CUF, the previous equation becomes:

$$
\delta L_{ext} = F_\tau N_i \mathbf{P} \delta \mathbf{q}_{\tau i}^T \tag{21}
$$

This last equation allows the identification od the components of the nucleus that have to be loaded, that is, it leads to the proper assembling of the loading vector by detecting the displacement variables that have to be loaded.

It should be noted that no assumptions on the expansion order have been made in formulating the stiffness matrix and the load vector. It is therefore possible to obtain refined beam models without changing the formal expression of the nucleus components. This is the key point of CUF which allows the implementation of any-order one-dimensional theories with only nine FORTRAN statements.

3. Results and Discussion

The enhanced capabilities of the present beam formulation when dealing with laminated box beams are demonstrated in this section. First, a laminated beam is considered in order to show the layer-wise characteristics of the LE CUF models. Both closed and open single-cell laminated box beams are subsequently addressed. The results by LE and, when possible, TE models are compared with those from the literature and with FE solutions by the commercial code MSC Nastran. Nastran models were build with CHEXA 8-noded solid elements and all the solutions provided result from convergence analyses. Unless differently specified, ten B4 elements were used along the beam axis in the case of CUF models.

Some benchmark results are also provided in the second part of this section, where two- and three-cell laminated box beams undergoing complex 3D strain/stress fields are finally analysed by the present LE beam models.

3.1. Eight-layer laminated beam

A cantilever beam composed by eight layers is considered as the first assessment. The geometric characteristics of the beam are shown in Fig. 5, together with the symmetric stacking sequence. The elastic modulus in the transversal direction (E_2=E_3), the shear moduli (G_{12} = G_{13} = G_{23}), and the Poissons ratios (ν_{12} = ν_{13} = ν_{23}) of the two orthotropic materials composing the lamina are assumed to be 1 GPa, 0.5 GPa and 0.25, respectively. In contrast, the Young modulus along the fiber direction of the material labeled with the number 1 is 30 GPa whereas the one related to material 2 is 5 GPa. The structure is loaded at the free end with a concentrated load equal to $F_z = -0.2$ N.

In Table 1, the vertical displacement at the tip and the normal stress component at (0.5, 45, 5) mm are given (the coordinates of the verification point are measured from the bottom left corner

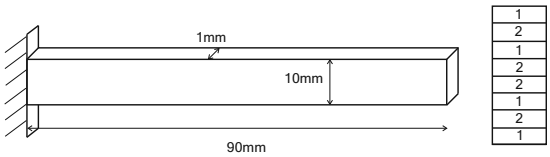

Figure 5: 8-layer laminated beam

Model	$-u_z \times 10^2$ (mm)	$\sigma_{yy} \times 10^3$ (MPa)	DOFs
Present TE and LE models			
TBM	2.988	730	155
$N = 3$	3.026	730	930
$N = 6$	3.028	730	2604
$N = 9$	3.028	730	5115
8 L9	3.029	730	4743
Reference solutions			
Nguyen and Surana [38]	3.031	720	
Davalos et al. [39]	3.029	700	
Xiaoshan [40]	3.060	750	
Carrera and Pagani [35]	3.026	731	6696
Carrera et al. [41]	3.040	729	1023

Table 1: Vertical displacement at the tip and normal stress at $(0.5, 45, 5)$ mm, 8-layer laminated beam

of the clamped section) along with the number of DOFs for each model. Classical TBM, up to the ninth-order ($N = 9$) TE as well as an 8 L9 LE models are shown in the table. In particular, the LE model is built by considering one single L9 element for each layer. The results by the present methodologies are compared with solutions from the literature [38, 39, 40] as well as with refined CUF models from [41, 35], where zig-zag theories and multi-line approaches were respectively employed.

The layer-wise capabilities of the present LE refined model are clearly evident from the analysis of the 8-layer beam and from the stress distributions given in Fig. 6, where the present beam models are compared to the analytical solution derived by the theory of elasticity presented in [42].

3.2. Single-cell box beams

Hollow rectangular cross-section laminated box beams are addressed here. The structure considered in this first analysis case was also used for experimental [43] and numerical [44, 45] investigations in previous works. The cross-section geometry is shown in Fig. 7. The dimensions of the beam are as follows: length $L = 762$ mm, height $h = 13.6$ mm, width $b = 24.2$ mm and thickness $t = 0.762$ mm. The box beam is made of six orthotropic layers with

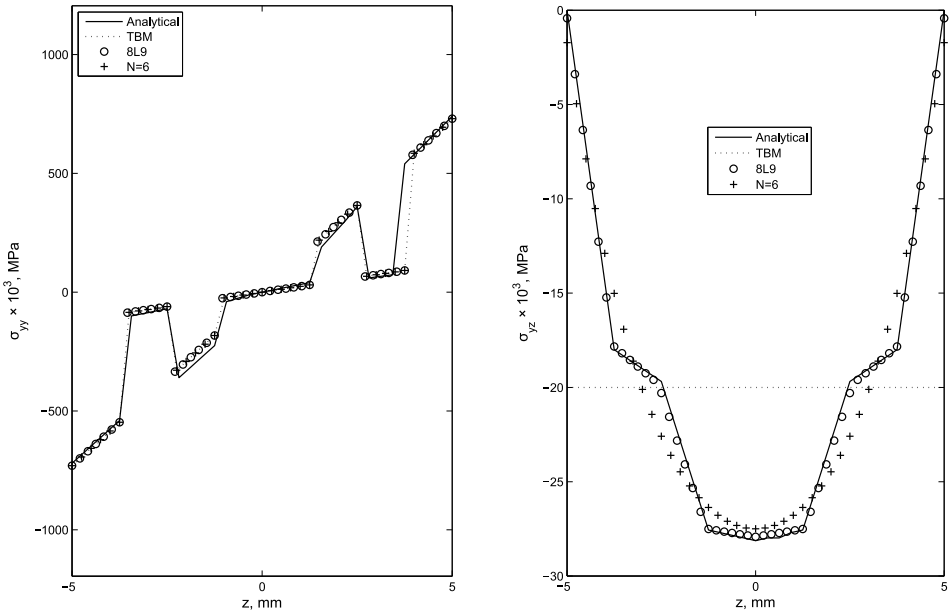

(a) σ_{yy} at y = 45 mm (b) σ_{yz} at y = 45 mm

Figure 6: Distribution of axial, σ_{yy}, and transverse shear, σ_{yz}, stresses for the 8-layer laminated beam

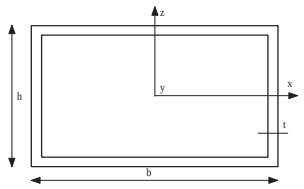

Figure 7: Cross-section of the composite box beam

the following material properties: $E_1 = 141.96$ GPa, $E_2 = E_3 = 9.79$ GPa, $\nu_{12} = \nu_{13} = 0.42$, $\nu_{23} = 0.5$, $G_{12} = G_{13} = 6.0$ GPa, $G_{23} = 4.83$ GPa. The six layers have the same thickness. CUS (Circumferentially Uniform Stiffness) stacking sequences are addressed and they are detailed in Table 2, where the same lamination schemes and the same notation as used in the literature papers are adopted. Clamped-free boundary conditions are considered and a 0.113 Nm tip torque is applied to the CUS2 and CUS3 lay-ups. The angle of twist distribution along the cantilever beam for CUS2 lay-up and for CUS3 lay-up are presented in Figs. 8.

Results from the sixth-order ($N = 6$) TE and a 24 L9 LE models are given in the figures

Lay-up	Flanges		Webs	
	Top	Bottom	Left	Right
CUS2	$[0°/30°]_3$	$[0°/-30°]_3$	$[0°/30°]_3$	$[0°/-30°]_3$
CUS3	$[0°/45°]_3$	$[0°/-45°]_3$	$[0°/45°]_3$	$[0°/-45°]_3$

Table 2: Various stacking sequences of the box beam used for comparison with previous works

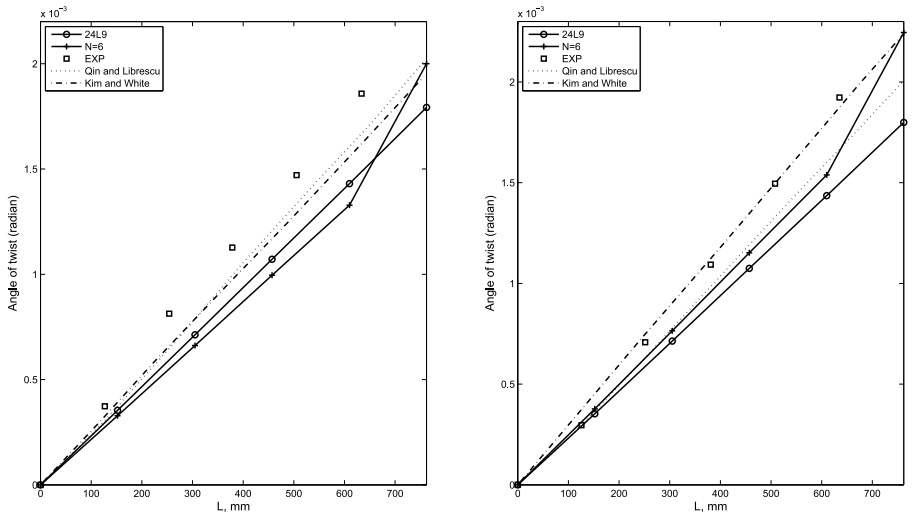

(a) CUS2 (b) CUS3

Figure 8: Variation of the angle of twist along the length of box beam.

and they are compared with the solutions from Qin and Librescu [45] and Kim and White [44] as well as with experimental tests by Chandra and Chopra [43]. Regarding the present 24 L9 model, it was obtained by using one single L9 element per layer on each flange and web. It can be concluded that the present beam formulations can deal with CUS lay-up box beam configurations. The results by the present LE and TE models are, in fact, in good agreement with those from numerical solutions and experimental data.

A cantilever composite box beam with $[0^\circ/90^\circ]$ lay-up for the webs and $[-45^\circ/+45^\circ]$ lay-up for the flanges is considered next, and it is hereinafter referred to as $[0^\circ/90^\circ/-45^\circ/+45^\circ]$ lay-up box beam. The cross-section geometry and dimension of the beam are same as presented in the previous analysis, see Fig. 7. The material properties are: $E_1 = 69.0$ GPa, $E_2 = E_3 = 10.0$ GPa, $\nu_{12} = \nu_{13} = \nu_{23} = 0.25$, $G_{12} = G_{13} = G_{23} = 6$ GPa. Two downwards point loads having the same magnitude ($F_z = -50$ N) are applied at two top corners of the beam at the tip cross-section. The resulting displacement and stress components are numerically obtained with the present TE and LE 1D theories and they are compared with a MSC Nastran 3D FE model (hereinafter referred to as SOLID). Three different aspect ratios are considered, $L/b = 10$, $L/b = 20$ and $L/b = 30$, and the results are shown in Table 3. Columns 4 and 5 give the results from the classical EBBM and TBM models. The TE model results are listed in the sixth ($N = 3$) and seventh ($N = 6$) columns. Column 8 represents the results from the LE model, which was obtained by using 16 L9 elements on the cross-section. Figure 9 shows the cross-sectional distribution of the L9

L/b			Classical models		TE		16 L9	SOLID
		$[x, y, z]$	EBBM	TBM	$N = 3$	$N = 6$		
	DOFs		155	600	930	2604	7740	360000
10	u_z	$[0, L, +h/2]$	7.09	7.15	7.09	7.16	7.16	7.17
	σ_{yy}	$[0, L/2, +h/2]$	85.24	85.27	84.44	85.30	85.80	85.4
	σ_{yy}	$[0, 0, +h/2]$	170.48	170.51	163.50	165.77	167.74	165.4
	σ_{yz}	$[b/2, L/2, +h/4]$	0	−6.40	−9.64	−8.94	−8.31	−8.93
20	u_z	$[0, L, +h/2]$	56.43	56.51	55.86	56.25	56.70	56.80
	σ_{yy}	$[0, L/2, +h/2]$	170.48	170.48	169.19	170.88	170.52	170.90
	σ_{yy}	$[0, 0, +h/2]$	340.96	340.96	331.75	332.18	336.49	338.10
	σ_{yz}	$[b/2, L/2, +h/4]$	0	−10.30	−14.74	−13.66	−12.11	−12.85
30	u_z	$[0, L, +h/2]$	191.45	191.71	189.39	190.59	191.85	191.28
	σ_{yy}	$[0, L/2, +h/2]$	255.72	255.72	253.92	256.71	256.23	256.37
	σ_{yy}	$[0, 0, +h/2]$	511.45	511.45	499.62	500.89	504.25	509.14
	σ_{yz}	$[b/2, L/2, +h/4]$	0	−14.21	−19.66	−18.36	−15.63	−16.77

Table 3: Displacement and stress components of the $[0°/90°/-45°/+45°]$ single-cell box beam undergoing two point loads

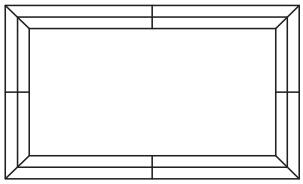

Figure 9: Cross-sectional distribution of L9 elements for the $[0°/90°/-45°/+45°]$ single-cell box beam

elements in the case of the LE model. Each rectangle in the figure represents a L9 element. The results from the MSC Nastran solid model are also given in Table 3, where the displacement and stress components measured at different location are shown together with the number of DOFs for each model implemented. The cross-sectional distribution of axial, σ_{yy} and shear stresses, σ_{yz}, above the mid-span cross-section of the $[0°/90°/-45°/+45°]$ short ($L/b = 10$) box beam are plotted in Fig. 10 and Fig. 11, respectively. Figure 12 finally shows the through-the-thickness variation of the axial stress, σ_{yy}, on the top flange and the variation of the shear stress, σ_{yz}, along the first layer on the right web at the mid-span cross-section.

A second loading case is also considered for the $[0°/90°0/-45°/+45°]$ single-cell box

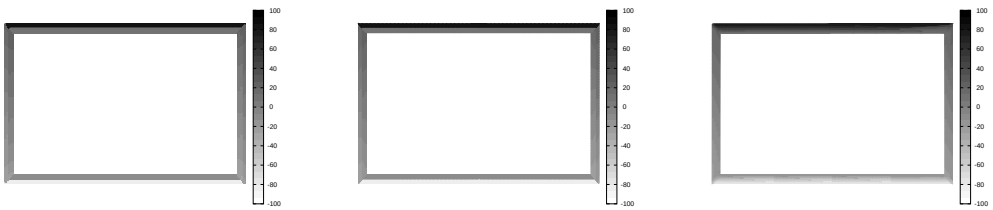

(a) $N = 6$ (b) 16 L9 (c) SOLID

Figure 10: Axial stress distribution, σ_{yy}, above the mid-span cross-section of the $[0°/90°/-45°/+45°]$ single-cell short ($L/b = 10$) box beam undergoing two point loads

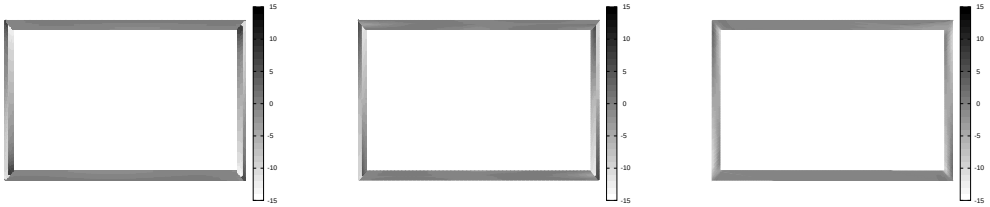

(a) $N = 6$ (b) 16 L9 (c) SOLID

Figure 11: Shear stress distribution, σ_{yz}, above the mid-span cross-section of the $[0°/90°/-45°/+45°]$ single-cell short ($L/b = 10$) box beam undergoing two point loads

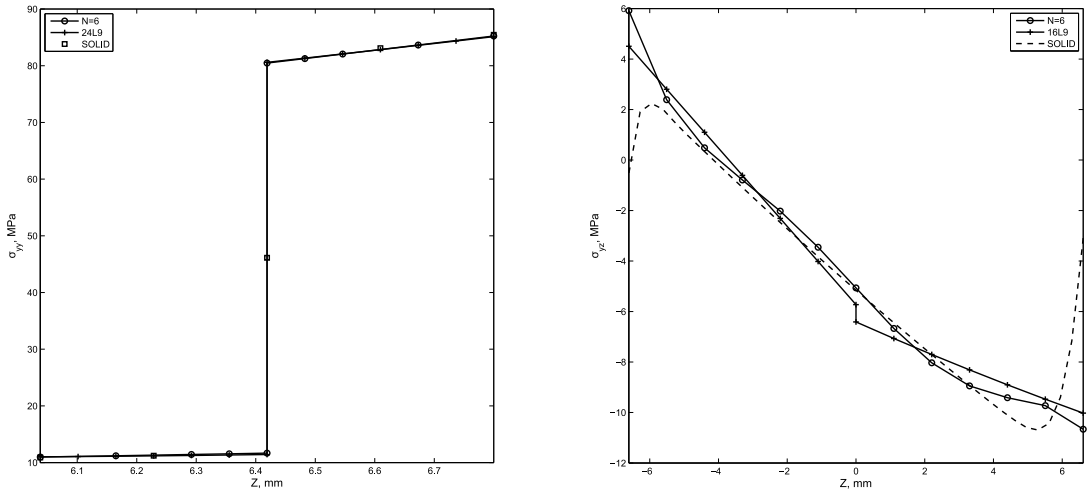

(a) (b)

Figure 12: Variation of the axial stress, σ_{yy}, along the thickness of the top flange (a) and variation of the shear stress, σ_{yz}, along the first layer of the right web (b). $[0°/90°/-45°/+45°]$ single-cell short ($L/b = 10$) box beam undergoing two point loads

L/b		$[x, y, z]$	$N = 6$	16 L9	SOLID
	DOFs		2604	7740	360000
10	u_z	$[0, L, +h/2]$	7.15	7.17	7.27
	σ_{yy}	$[0, L/2, +h/2]$	85.12	85.60	85.4
	σ_{yy}	$[0, 0, +h/2]$	164.04	164.58	165.0
	σ_{yz}	$[b/2, L/2, +h/4]$	−11.78	−10.72	−11.64
20	u_z	$[0, L, +h/2]$	56.25	56.70	56.80
	σ_{yy}	$[0, L/2, +h/2]$	170.70	170.65	170.96
	σ_{yy}	$[0, 0, +h/2]$	331.89	334.65	336.13
	σ_{yz}	$[b/2, L/2, +h/4]$	−16.74	−14.45	−15.63
30	u_z	$[0, L, +h/2]$	190.59	190.84	191.20
	σ_{yy}	$[0, L/2, +h/2]$	256.45	256.40	256.41
	σ_{yy}	$[0, 0, +h/2]$	500.31	503.12	507.40
	σ_{yz}	$[b/2, L/2, +h/4]$	−21.65	−17.93	−19.56

Table 4: Displacement and stress components of the $[0°/90°/-45°/+45°]$ single-cell box beam undergoing one point load

beam in order to demonstrate the capabilities of the present methodology to deal with flexural-torsional phenomena. A point load $F_z = -100$ N is applied at top right corner at the tip cross-section. Displacement and stress values at different locations by different models are given in Table 4. The following comments can be made:

- Classical models give acceptable results in terms of displacements when pure bending loads are applied.
- Higher-order models are necessary if stress distributions are required and coupled flexural-torsional phenomena are involved.
- Refined TE and LE models are able to reproduce 3D-like results with very low computational costs.

3.3. Single-cell box beam with open cross-section

In order to underline the enhanced capabilities of the present beam formulation, the same $[0°/90°/-45°/+45°]$ single-cell box beam of the previous analysis case with a cut at bottom edge and along the whole length is considered, see Fig. 13. As in the previous analysis, the first load case deals with two point loads $F_z = -50$ N applied at two top corners at the tip cross-section. Displacement and stress values at different locations are presented in Table 5. The results from TE models are not given in Table 5 since, as it was shown in recent works [36, 18], they cannot deal with cross-sectional cuts. In fact, the results by the TE models for the

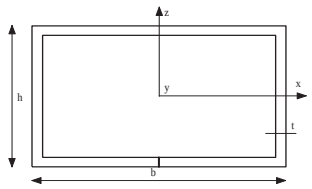

Figure 13: Cross-section of the laminated box beam with cut

L/b		$[x,y,z]$	16 L9	Solid
	DOFs		7905	379560
10	u_z	$[0,L,+h/2]$	7.94	8.06
	σ_{yy}	$[0,L/2,+h/2]$	86.93	87.23
	σ_{yy}	$[0,0,+h/2]$	167.97	165.80
	σ_{yz}	$[b/2,L/2,+h/4]$	-7.07	-7.50
20	u_z	$[0,L,+h/2]$	57.56	57.80
	σ_{yy}	$[0,L/2,+h/2]$	169.88	170.80
	σ_{yy}	$[0,0,+h/2]$	338.39	339.70
	σ_{yz}	$[b/2,L/2,+h/4]$	-12.12	-12.96
30	u_z	$[0,L,+h/2]$	192.05	192.50
	σ_{yy}	$[0,L/2,+h/2]$	254.82	255.60
	σ_{yy}	$[0,0,+h/2]$	507.26	512.01
	σ_{yz}	$[b/2,L/2,+h/4]$	-15.78	-17.11

Table 5: Displacement and stress components of the $[0°/90°/-45°/+45°]$ single-cell box beam with cut undergoing two point loads

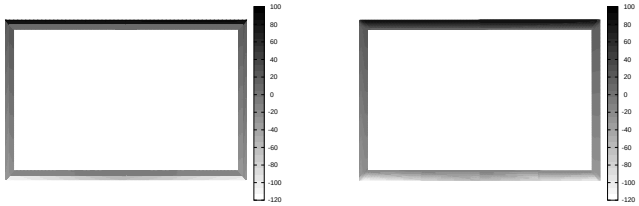

(a) 16 $L9$ (b) SOLID

Figure 14: Axial stress distribution, σ_{yy}, above the mid-span cross-section of the $[0°/90°/-45°/+45°]$ single-cell short ($L/b = 10$) box beam with cut undergoing two point loads

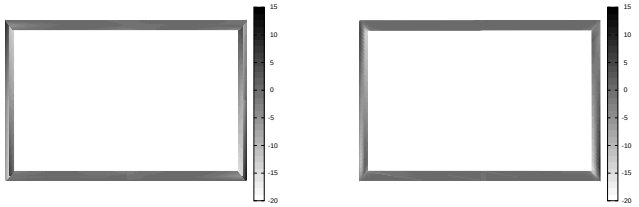

(a) 16 $L9$ (b) SOLID

Figure 15: Shear stress distribution, σ_{yz}, above the mid-span cross-section of the $[0°/90°/-45°/+45°]$ single-cell short ($L/b = 10$) box beam with cut undergoing two point loads

single-cell box beam with the cut are very close to those presented in Table 3, where the same structure without the cut was considered. The cross-sectional distribution of the axial stress, σ_{yy}, and shear stress, σ_{yz}, at middle of the beam are plotted in Fig. 14 and Fig. 15, respectively.

In the second load case, a single point load $F_z = -100$ N was applied at the top right cornet on the tip cross-section. The results by the present 16 L9 model are given in Table 6 and they are compared to the 3D MSC Nastran model. For both the 3D model and the LE one, the cut is realized by un-connecting the superimposed nodes at the cut interface. The following conclusions hold:

- Both classical models and refined TE models are not able to deal with laminated box beams with cuts on the cross-sections. The former, in fact, cannot foresee any cross-sectional deformation. The latter would require very high orders of expansion, whose high number of DOFs might not justify the adoption of a beam model.

- The results suggest that the present LE 1D model can deal with laminated beams with cuts. In fact, the results by the LE model are in good agreement with those from the MSC Nastran solid solution and very low DOFs are used by the former.

L/b		$[x, y, z]$	16 L9	SOLID
	DOFs		7905	379560
10	u_z	$[0, L, +h/2]$	7.98	8.11
	σ_{yy}	$[0, L/2, +h/2]$	85.77	85.70
	σ_{yy}	$[0, 0, +h/2]$	165.42	163.20
	σ_{yz}	$[b/2, L/2, +h/4]$	−15.43	−16.19
20	u_z	$[0, L, +h/2]$	57.65	57.80
	σ_{yy}	$[0, L/2, +h/2]$	164.65	165.47
	σ_{yy}	$[0, 0, +h/2]$	337.48	337.40
	σ_{yz}	$[b/2, L/2, +h/4]$	−29.19	−30.70
30	u_z	$[0, L, +h/2]$	192.17	192.60
	σ_{yy}	$[0, L/2, +h/2]$	245.37	246.10
	σ_{yy}	$[0, 0, +h/2]$	506.76	509.90
	σ_{yz}	$[b/2, L/2, +h/4]$	−40.72	−43.34

Table 6: Displacement and stress components of the $[0°/90°/-45°/+45°]$ single-cell box beam with cut undergoing one-point load

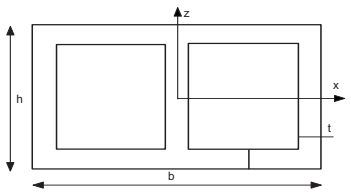

Figure 16: Cross-section of the two-cell box beam

3.4. Multi-cell laminated box beams

Given the accuracy of the proposed LE modelling technique in dealing with laminated box beams, some benchmark results about multi-cell structures are provided in this section. First, a composite two-cell beam, whose cross-section is shown in Fig. 16, is considered. The structure undergoes clamped-free boundary conditions and a cut is placed in correspondence of the bottom edge of the right cell as shown in Fig. 16. The geometric dimensions, the lamination sequence $[0°/90°/-45°/+45°]$ (i.e. $[0°/90°]$ lay-up for the vertical edges and $[-45°/+45°]$ lay-up for horizontal edges), and the material properties are same as in the previous analysis cases. Two vertical and two horizontal point loads are applied. In particular, the two vertical forces ($F_z = 50$ N) are directed upwards and they are applied at the two corners of the top flange at the tip cross-section. On the other hand, the two horizontal loads have the same magnitude but opposite directions: The load applied at the bottom right corner has the same direction as the x-axis ($F_x = 50$ N), whereas the the load applied and the bottom left corner is directed towards the negative values of the x-axis ($F_x = -50$ N). Displacement and stress values at different lo-

L/b		$[x, y, z]$	22 L9
	DOFs		10602
10	u_z	$[0, L, +h/2]$	6.48
	σ_{yy}	$[0, L/2, +h/2]$	−78.32
	σ_{yy}	$[0, 0, +h/2]$	−181.39
	σ_{yz}	$[b/2, L/2, -h/4]$	8.82

Table 7: Displacement and stress components for the $[0°/90°/-45°/+45°]$ two-cell box beam

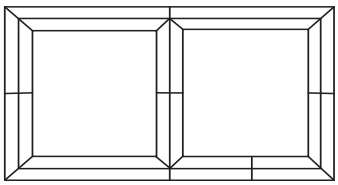

Figure 17: Cross-sectional distribution of L9 elements for the $[0°/90°/-45°/+45°]$ two-cell box beam

cations are presented in Table 7 for a beam aspect ratio equal to $L/b = 10$. Table 7 refers to the solution from a 22 L9 LE model, whose cross-sectional discretization is shown in Fig. 17. The cross-sectional distributions of stress components on the mid-span cross-section of the beam are shown in Fig. 18. The deformed configuration of the structure under consideration is also shown in Fig. 19 in order to highlight that complex 3D strain fields can be captured with the present models.

A cantilever three-cell composite box beam is finally considered as the last analysis, see Fig. 20. A cut is realised at the middle of the bottom edge along the whole length of the beam. The geometric dimensions (h, b, t), the lamination sequence $[0°/90°/-45°/+45°]$ and the material properties are the same as those of the previous analyses. The same loading condition considered in the case of the two-cell box beam is adopted and the results by a 22 L9 model (Fig. 21) are shown in Table 8. Cross-sectional stress distributions at middle of the beam are

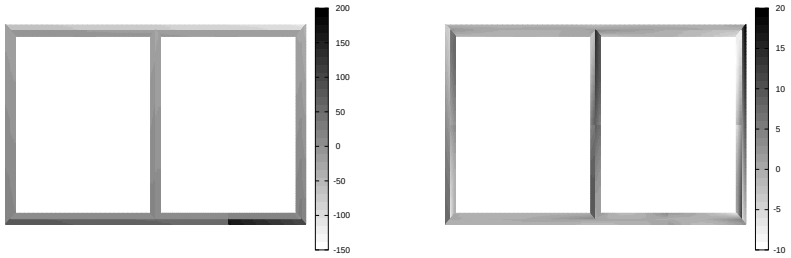

(a) σ_{yy} (b) σ_{yz}

Figure 18: Axial and shear stress distributions above the mid-span cross-section of the $[0°/90°/-45°/+45°]$ two-cell short ($L/b = 10$) box beam

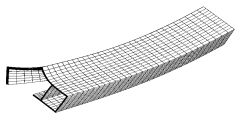

Figure 19: Deformed configuration of the $[0°/90°/-45°/+45°]$ two-cell short ($L/b = 10$) box beam

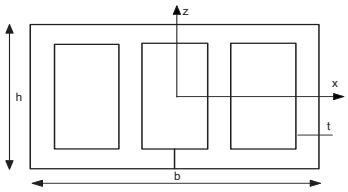

Figure 20: Cross-section of the three-cell box beam

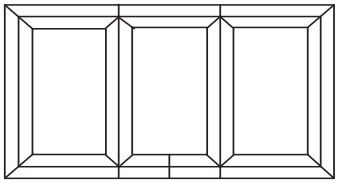

Figure 21: Cross-sectional distribution of L9 elements for the $[0°/90°/-45°/+45°]$ three-cell box beam

L/b		$[x, y, z]$	22 L9
	DOFs		10602
10	u_z	$[0, L, +h/2]$	6.54
	σ_{yy}	$[0, L/2, +h/2]$	−81.75
	σ_{yy}	$[0, 0, +h/2]$	−152.43
	σ_{yz}	$[b/2, L/2, 0]$	8.44

Table 8: Displacement and stress components for the $[0°/90°/-45°/+45°]$ two-cell box beam

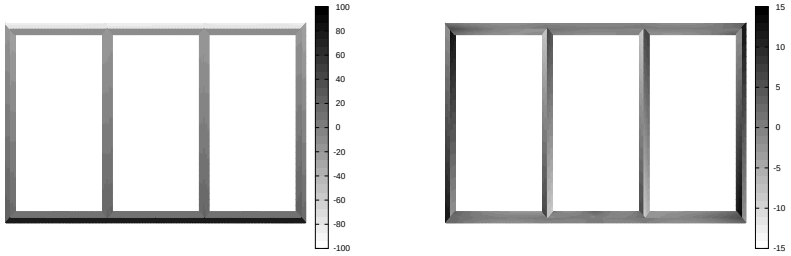

(a) σ_{yy} (b) σ_{yz}

Figure 22: Axial and shear stress distributions above the mid-span cross-section of the $[0°/90°/-45°/+45°]$ three-cell short ($L/b = 10$) box beam

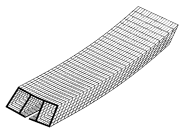

Figure 23: Deformed configuration of the $[0°/90°/-45°/+45°]$ three-cell short ($L/b = 10$) box beam

plotted in Fig. 22. The 3D deformed configuration of the beam is finally shown in Fig. 23.

4. Conclusion

Static analyses of laminated box beams have been presented in this paper. The Carrera Unified Formulation (CUF) has been used to hierarchically enrich one-dimensional (1D) kinematic fields by arbitrary cross-sectional functions. The principle of virtual displacement has been subsequently employed along with CUF to formulate finite element (FE) arrays in terms of fundamental nuclei, which either do not depend on the expansion order or on the class of the beam model. In fact, two different classes have been formulated and they have been referred to as TE (Taylor Expansion) and LE (Lagrange Expansion). TE models exploit Taylor-like polynomials as cross-sectional functions. On the other hand, Lagrange polynomials are used in the case of LE, which therefore exhibits layer-wise capabilities. Various assessments have been proposed through the present work, and the results by both TE and LE refined 1D CUF models have been compared with the results available from the literature and with the solutions from the FE commercial code MSC Nastran. The enhanced modelling characteristics of the present models when dealing with laminated box beams have been widely confirmed, especially for LE models, which are able to reproduce solid-like analysis with very low computational efforts. Furthermore, given the accuracy of the present LE approach, some benchmark results about multi-cell

laminated box beams have also been provided in order to fill a gap in the research literature.

References

[1] L. Euler, De curvis elasticis, Lausanne and Geneva: Bousquet, 1744.

[2] S. P. Timoshenko, On the transverse vibrations of bars of uniform cross section, Philosophical Magazine 43 (1922) 125–131.

[3] O. Bauchau, B. Coffenberry, L. Rehfield, Composite box beam analysis: Theory and experiments, Journal of Reinforced Plastics and Composites 6 (1987) 25–35, dOI: 10.1177/073168448700600103.

[4] J. Loughlan, M. Ata, The behaviours of open and closed section carbon fibre composite beams subjected to constrained torsion, Composite Structures 38 (1) (1997) 631–647.

[5] J. Loughlan, M. Ata, The constrained torsional characteristics of some carbon fibre composite box-beams, Thin-Walled Structures 28 (1997) 233–252.

[6] J. Loughlan, M. Ata, The analysis of carbon fibre composite box beams subjected torsion with variable twist, Comput. Methods Appl. Mech. Engrg. 152 (1998) 373–391.

[7] J. Loughlan, M. Ahmed, Multi-cell carbon fibre composite box beams subjected to torsion with variable twist, Thin-Walled Structures 46 (2008) 914–924.

[8] A. Stemple, S. Lee, Large deflection static and dynamic finite element analysis of composite beams with arbitrary cross-sectional warping, In: proceeding of the AIAA/ASME/ASCE/AHS/ASC 30th Structures, Structural Dynamics and Materials Conference Washington (1989) 1788–98.

[9] R. Chandra, A. Stemple, I. Chopra, Thin-walled composite beams under bending, torsional, and extensional loads, J. Aircrafts 27 (7) (1990) 619–626.

[10] M. Mitra, S. Gopalakrishnan, M. Seetharama Bhat, A new super convergent thin walled composite beam element for analysis of box beam structures, International Journal of Solids and Structures 41 (2004) 1491–1518, dOI: 10.1016/j.ijsolstr.2003.10.024.

[11] A. Sheikh, O. Thomsen, An efficient beam element for the analysis of laminated composite beams of thin-walled open and closed cross sections, Composites Science and Technology 68 (2008) 2273–2281, dOI: 10.1016/j.compscitech.2008.04.018.

[12] T. P. Vo, J. Lee, Flexuraltorsional behavior of thin-walled closed-section composite box beams, Engineering Structures 29 (2007) 1774–1782, dOI:10.1016/j.engstruct.2006.10.002.

[13] T. P. Vo, J. Lee, N. Ahn, On sixfold coupled vibrations of thin-walled composite box beams, Composite Structures 89 (2009) 524–535, dOI:10.1016/j.compstruct.2008.11.004.

[14] T. P. Vo, J. Lee, Flexuraltorsional buckling of thin-walled composite box beams, Thin-Walled Structures 45 (2007) 790–798, dOI:10.1016/j.tws.2007.06.001.

[15] R. Suresh, S. Malhotra, Some studies on static analysis of composite thin-walled box beam, Computers & Structures 62 (4) (1995) 625–634.

[16] A. Genoese, A. Genoese, A. Bilotta, G. Garcea, A composite beam model including variable warping effects derived from a generalized saint venant solution, Composite Structures 110 (2014) 140–151, dOI:10.1016/j.compstruct.2013.11.020.

[17] A. Genoese, A. Genoese, A. Bilotta, G. Garcea, A generalized model for heterogeneous and anisotropic beams including section distortions, Thin-Walled Structures 74 (2014) 85–103, dOI:10.1016/j.tws.2013.09.019.

[18] E. Carrera, M. Filippi, P. K. Mahato, A. Pagani, Advanced models for free vibration analysis of laminated beams with compact and thin-walled open/closed sections, Journal of Composite MaterialsDOI:10.1177/0021998314541570.

[19] E. Carrera, G. Giunta, M. Petrolo, Beam Structures: Classical and Advanced Theories, John Wiley, 2011, dOI: 10.1002/9781119978565.

[20] E. Carrera, G. Giunta, P. Nali, M. Petrolo, Refined beam elements with arbitrary cross-section geometries, Computers and Structures 88 (5–6) (2010) 283–293, dOI: 10.1016/j.compstruc.2009.11.002.

[21] E. Carrera, M. Petrolo, E. Zappino, Performance of cuf approach to analyze the structural behavior of slender bodies., Journal of Structural Engineeing 138 (2) (2012) 285–297.

[22] E. Carrera, M. Petrolo, P. Nali, Unified formulation applied to free vibrations finite element analysis of beams with arbitrary section, Shock and Vibrations 18 (3) (2011) 485–502.

[23] E. Carrera, M. Petrolo, A. Varello, Advanced beam formulations for free vibration analysis of conventional and joined wings, Journal of Aerospace Engineering 25 (2) (2012) 282–293.

[24] E. Carrera, M. Filippi, E. Zappino, Free vibration analysis of thin-walled cylinders reinforced with longitudinal and transversal stiffeners, Journal of Vibration and Acoustics - ASME DC 135 (1), dOI:http://dx.doi.org/10.1115/1.4007559.

[25] A. Pagani, E. Carrera, M. Boscolo, J. Banerjee, Refined dynamic stiffness elements applied to free vibration analysis of generally laminated composite beams with arbitrary boundary conditions, Composite Structures 110 (2014) 305–316.

[26] A. Pagani, E. Carrera, J. Banerjee, P. Cabral, G. Caprio, A. Prado, Free vibration analysis of composite plates by higher-order 1d dynamic stiffness elements and experiments, Composite Structures 118 (2014) 654–663, dOI: /10.1016/j.compstruct.2014.08.020.

[27] E. Carrera, M. Filippi, E. Zappino, Analysis of rotor dynamic by one-dimensional variable kinematic theories, Journal of Engineering for Gas Turbines and Power - ASME DC 135 (9) (2013) 092501–09.

[28] E. Carrera, M. Filippi, E. Zappino, Free vibration analysis of rotating composite blades via carrera unified formulation, Composite Structures 106 (2013) 317–325, dOI:http://dx.doi.org/10.1016/j.compstruct.2013.05.055.

[29] E. Carrera, M. Filippi, Variable kinematic one-dimensional finite elements for the analysis of rotors made of composite materials, Journal of Engineering for Gas Turbines and Power - ASMEDOI: 10.1115/1.4027192.

[30] E. Carrera, Developments, ideas, and evaluations based upon reissners mixed variational theorem in the modeling of multilayered plates and shells, Appl. Mech. Rev. 54 (4) (2001) 301–329.

[31] E. Carrera, M. Petrolo, Refined one-dimensional formulations for laminated structure analysis, AIAA Journal 50 (1) (2012) 176–189, dOI: 10.2514/1.J051219.

[32] E. Carrera, A. Pagani, M. Petrolo, Classical, refined and component-wise theories for static analysis of reinforced-shell wing structures, AIAA Journal 51 (5) (2013) 12551268, dOI: 10.2514/1.J052331.

[33] E. Carrera, A. Pagani, M. Petrolo, Component-wise method applied to vibration of wing structures, Journal of Applied Mechanics 80 (2013) 041012, dOI: 10.1115/1.4007849.

[34] E. Carrera, A. Pagani, M. Petrolo, Refined 1d finite elements for the analysis of secondary, primary and complete civil engineering structures, Journal of Structural EngineeringIn Press.

[35] E. Carrera, A. Pagani, Multi-line enhanced beam model for the analysis of laminated composite structures, Composites: Part B 57 (2014) 112–119, http://dx.doi.org/10.1016/j.compositesb.2013.09.046.

[36] E. Carrera, M. Petrolo, Refined beam elements with only displacement variables and plate/shell capabilities, Meccanica 47 (3) (2012) 537–556, dOI: 10.1007/s11012-011-9466-5.

[37] K. Bathe, Finite element procedure, Prentice hall, 1996.

[38] K. Surana, S. Nguyen, Two-dimensional curved beam element with higher-order hierarchical transverse approximation for laminated composites, Composite Structures 36 (1990) 499–511.

[39] J. F. Davalos, Y. Kim, E. J. Barbero, Analysis of laminated beams with a layerwise constant shear theory, Composite Structure 28 (1994) 241–53.

[40] Y. Z. Xiaoshan Lin, A novel one-dimensional two-node shear-flexible layered composite beam element, Finite Element Analysis and Design 47 (2011) 676–82.

[41] E. Carrera, M. Filippi, E. Zappino, Laminated beam analysis by polynomial, trigonometric, exponential and zig-zag theories, European Journal of Mechanics ASolids 41 (2013) 58–69.

[42] S. Lekhnitskii, Anisotropic Plates, 2nd Edition, Translated from the 2nd Russian Edited by SW Tsai and Cheron, Bordon and Breach, 1968, translated from 2nd Russian Edition.

[43] R. Chandra, I. Chopra, Experimental-theoretical investigation of the vibration characteristics of rotating composite box beam, J. Aircrafts 29 (4) (1992) 657–64.

[44] C. Kim, S. R. White, Thick-walled composite beam theory including 3-D elastic effects and torsional warping, International Journal of Solid Structures 34 (31-32) (1997) 4237–4259.

[45] Z. Qin, L. Librescu, On a shear-deformable theory of anisotropic thin-walled beams: further contribution and validations, Composite Structures 56 (2002) 345–358.

Appendix A

For a cross-section made of non-homogeneous orthotropic material, the components of the fundamental nucleus $\boldsymbol{K}^{ij\tau s}$ are here written:

$$
\begin{aligned}
K_{xx} = {} & I_l^{i,y\,j} \triangleleft F_\tau \tilde{C}_{46} F_{s,z} \triangleright + I_l^{i,y\,j} \triangleleft F_\tau \tilde{C}_{26} F_{s,x} \triangleright + I_l^{i,y\,j,y} \triangleleft F_\tau \tilde{C}_{66} F_s \triangleright + \\
& I_l^{ij} \triangleleft F_{\tau,z} \tilde{C}_{44} F_{s,z} \triangleright + I_l^{ij} \triangleleft F_{\tau,z} \tilde{C}_{24} F_{s,x} \triangleright + I_l^{ij,y} \triangleleft F_{\tau,z} \tilde{C}_{46} F_s \triangleright + \\
& I_l^{ij,y} \triangleleft F_{\tau,x} \tilde{C}_{26} F_s \triangleright + I_l^{ij} \triangleleft F_{\tau,x} \tilde{C}_{24} F_{s,z} \triangleright + I_l^{ij} \triangleleft F_{\tau,x} \tilde{C}_{22} F_{s,x} \triangleright \\
K_{xy} = {} & I_l^{i,y\,j} \triangleleft F_\tau \tilde{C}_{66} F_{s,x} \triangleright + I_l^{i,y\,j} \triangleleft F_\tau \tilde{C}_{56} F_{s,z} \triangleright + I_l^{i,y\,j,y} \triangleleft F_\tau \tilde{C}_{36} F_s \triangleright + \\
& I_l^{ij} \triangleleft F_{\tau,x} \tilde{C}_{26} F_{s,x} \triangleright + I_l^{ij} \triangleleft F_{\tau,x} \tilde{C}_{25} F_{s,z} \triangleright + I_l^{ij} \triangleleft F_{\tau,z} \tilde{C}_{46} F_{s,x} \triangleright + \\
& I_l^{ij} \triangleleft F_{\tau,z} \tilde{C}_{45} F_{s,z} \triangleright + I_l^{ij,y} \triangleleft F_{\tau,z} \tilde{C}_{43} F_s \triangleright + I_l^{ij,y} \triangleleft F_{\tau,x} \tilde{C}_{23} F_s \triangleright \\
K_{xz} = {} & I_l^{i,y\,j} \triangleleft F_\tau \tilde{C}_{46} F_{s,x} \triangleright + I_l^{i,y\,j} \triangleleft F_\tau \tilde{C}_{16} F_{s,z} \triangleright + I_l^{i,y\,j,y} \triangleleft F_\tau \tilde{C}_{56} F_s \triangleright + \\
& I_l^{ij} \triangleleft F_{\tau,z} \tilde{C}_{44} F_{s,x} \triangleright + I_l^{ij} \triangleleft F_{\tau,z} \tilde{C}_{14} F_{s,z} \triangleright + I_l^{ij} \triangleleft F_{\tau,x} \tilde{C}_{24} F_{s,x} \triangleright + \\
& I_l^{ij} \triangleleft F_{\tau,x} \tilde{C}_{21} F_{s,z} \triangleright + I_l^{ij,y} \triangleleft F_{\tau,z} \tilde{C}_{45} F_s \triangleright + I_l^{ij,y} \triangleleft F_{\tau,x} \tilde{C}_{25} F_s \triangleright \\
K_{yx} = {} & I_l^{ij,y} \triangleleft F_{\tau,x} \tilde{C}_{66} F_s \triangleright + I_l^{ij,y} \triangleleft F_{\tau,z} \tilde{C}_{56} F_s \triangleright + I_l^{i,y\,j} \triangleleft F_\tau \tilde{C}_{43} F_{s,z} \triangleright + \\
& I_l^{i,y\,j} \triangleleft F_\tau \tilde{C}_{23} F_{s,x} \triangleright + I_l^{i,y\,j,y} \triangleleft F_\tau \tilde{C}_{36} F_s \triangleright + I_l^{ij} \triangleleft F_{\tau,x} \tilde{C}_{46} F_{s,x} \triangleright + \\
& I_l^{ij} \triangleleft F_{\tau,x} \tilde{C}_{26} F_{s,x} \triangleright + I_l^{ij} \triangleleft F_{\tau,z} \tilde{C}_{45} F_{s,z} \triangleright + I_l^{ij} \triangleleft F_{\tau,z} \tilde{C}_{25} F_{s,x} \triangleright \\
K_{yy} = {} & I_l^{ij} \triangleleft F_{\tau,x} \tilde{C}_{66} F_{s,x} \triangleright + I_l^{ij} \triangleleft F_{\tau,x} \tilde{C}_{56} F_{s,z} \triangleright + I_l^{ij} \triangleleft F_{\tau,z} \tilde{C}_{56} F_{s,x} \triangleright + \\
& I_l^{ij} \triangleleft F_{\tau,z} \tilde{C}_{55} F_{s,z} \triangleright + I_l^{ij,y} \triangleleft F_{\tau,x} \tilde{C}_{36} F_s \triangleright + I_l^{ij,y} \triangleleft F_{\tau,z} \tilde{C}_{35} F_s \triangleright + \\
& I_l^{i,y\,j} \triangleleft F_\tau \tilde{C}_{36} F_{s,x} \triangleright + I_l^{i,y\,j} \triangleleft F_\tau \tilde{C}_{35} F_{s,z} \triangleright + I_l^{i,y\,j,y} \triangleleft F_\tau \tilde{C}_{33} F_s \triangleright \\
K_{yz} = {} & I_l^{ij} \triangleleft F_{\tau,x} \tilde{C}_{46} F_{s,x} \triangleright + I_l^{ij} \triangleleft F_{\tau,x} \tilde{C}_{16} F_{s,z} \triangleright + I_l^{ij} \triangleleft F_{\tau,z} \tilde{C}_{45} F_{s,x} \triangleright + \\
& I_l^{ij} \triangleleft F_{\tau,z} \tilde{C}_{15} F_{s,z} \triangleright + I_l^{ij,y} \triangleleft F_{\tau,x} \tilde{C}_{56} F_s \triangleright + I_l^{ij,y} \triangleleft F_{\tau,z} \tilde{C}_{55} F_s \triangleright + \\
& I_l^{i,y\,j} \triangleleft F_\tau \tilde{C}_{43} F_{s,x} \triangleright + I_l^{i,y\,j} \triangleleft F_\tau \tilde{C}_{13} F_{s,z} \triangleright + I_l^{i,y\,j,y} \triangleleft F_\tau \tilde{C}_{35} F_s \triangleright \\
K_{zx} = {} & I_l^{i,y\,j} \triangleleft F_\tau \tilde{C}_{45} F_{s,z} \triangleright + I_l^{i,y\,j} \triangleleft F_\tau \tilde{C}_{25} F_{s,x} \triangleright + I_l^{i,y\,j,y} \triangleleft F_\tau \tilde{C}_{56} F_s \triangleright + \\
& I_l^{ij} \triangleleft F_{\tau,x} \tilde{C}_{44} F_{s,z} \triangleright + I_l^{ij} \triangleleft F_{\tau,x} \tilde{C}_{24} F_{s,x} \triangleright + I_l^{ij} \triangleleft F_{\tau,z} \tilde{C}_{21} F_{s,x} \triangleright + \\
& I_l^{ij} \triangleleft F_{\tau,z} \tilde{C}_{14} F_{s,z} \triangleright + I_l^{ij,y} \triangleleft F_{\tau,x} \tilde{C}_{46} F_s \triangleright + I_l^{ij,y} \triangleleft F_{\tau,z} \tilde{C}_{16} F_s \triangleright
\end{aligned}
$$

$$
\begin{aligned}
K_{zy} = \; & I_l^{i,yj} \triangleleft F_\tau \tilde{C}_{56} F_{s,x} \triangleright \; + \; I_l^{i,yj} \triangleleft F_\tau \tilde{C}_{55} F_{s,z} \triangleright \; + \; I_l^{i,yj_y} \triangleleft F_\tau \tilde{C}_{35} F_s \triangleright \; + \\
& I_l^{ij} \triangleleft F_{\tau,z} \tilde{C}_{16} F_{s,z} \triangleright \; + \; I_l^{ij} \triangleleft F_{\tau,z} \tilde{C}_{15} F_{s,z} \triangleright \; + \; I_l^{ij} \triangleleft F_{\tau,x} \tilde{C}_{46} F_{s,x} \triangleright \; + \\
& I_l^{ij} \triangleleft F_{\tau,x} \tilde{C}_{45} F_{s,z} \triangleright \; + \; I_l^{ij_y} \triangleleft F_{\tau,x} \tilde{C}_{43} F_s \triangleright \; + \; I_l^{ij_y} \triangleleft F_{\tau,z} \tilde{C}_{13} F_s \triangleright
\end{aligned}
$$

$$
\begin{aligned}
K_{zz} = \; & I_l^{i,yj} \triangleleft F_\tau \tilde{C}_{45} F_{s,x} \triangleright \; + \; I_l^{i,yj} \triangleleft F_\tau \tilde{C}_{15} F_{s,z} \triangleright \; + \; I_l^{i,yj_y} \triangleleft F_\tau \tilde{C}_{55} F_s \triangleright \; + \\
& I_l^{ij} \triangleleft F_{\tau,x} \tilde{C}_{44} F_{s,x} \triangleright \; + \; I_l^{ij} \triangleleft F_{\tau,x} \tilde{C}_{14} F_{s,z} \triangleright \; + \; I_l^{ij} \triangleleft F_{\tau,z} \tilde{C}_{14} F_{s,x} \triangleright \; + \\
& I_l^{ij} \triangleleft F_{\tau,z} \tilde{C}_{11} F_{s,z} \triangleright \; + \; I_l^{ij_y} \triangleleft F_{\tau,x} \tilde{C}_{45} F_s \triangleright \; + \; I_l^{ij_y} \triangleleft F_{\tau,z} \tilde{C}_{15} F_s \triangleright
\end{aligned}
$$